

A New Planar Single-Channel Shim Coil Using Multiple Circular Currents for Magnetic Resonance Imaging

Daiki Tamada*, Katsumi Kose, and Tomoyuki Haishi¹

Institute of Applied Physics, University of Tsukuba, Tsukuba, Ibaraki 305-8573, Japan

¹*MRTechnology, Inc., Tsukuba, Ibaraki 305-8573, Japan*

Received March 27, 2012; accepted April 5, 2012; published online April 20, 2012

We propose a new planar single-channel shim coil for magnetic resonance imaging (MRI) permanent magnets. The coil design is based on the superposition of multiple circular currents and the stream function method. The designed shim coil was implemented for a permanent magnet with 1.0 T and a 90 mm gap. When the shim coil current was optimized, the magnetic field inhomogeneity decreased from 240 to 97 ppm (peak-to-peak) in the central cylindrical area (54.6 mm diameter, 60.0 mm height), demonstrating that the single-channel shim coil proposed here is a useful device for permanent narrow-gap magnets with complicated magnetic field distribution. © 2012 The Japan Society of Applied Physics

Magnetic field homogeneity is essential for acquiring high-quality magnetic resonance images and is achieved using magnetic field shimming. There are two major shimming methods, passive and active.

Passive shimming¹⁾ is performed by attaching pieces of magnetic material onto the magnet. This method is widely used because it has a reasonable cost and does not require a power supply. However, if a highly homogeneous magnetic field is required, attaching hundreds of magnetic material pieces to the magnet is time consuming.

Active shimming²⁾ uses shim coils with adjustable currents to cancel the magnetic field inhomogeneity. The spatial distribution of the magnetic field can be expressed as a superposition of orthogonal spatial functions, such as spherical harmonics, and for this reason, shim coils are frequently designed to generate the magnetic fields, each corresponding to one of the spherical harmonics.^{3,4)} Therefore, many shim coils are required to correct magnetic inhomogeneities up to their higher-order terms. Using multiple shim coils requires a power supply for each coil and consumes the gap or bore space of the magnet. Therefore, active shimming has problems in installation on a narrow-gap or small-bore magnet.

To solve these problems, we proposed a planar single-channel shim coil for a permanent magnet⁵⁾ using the target-field approach.^{6–8)} However, as is well known, the target-field approach has a design limitation.⁹⁾ To overcome this limitation, we proposed a single-channel shim coil based on the superposition of second-order shim coils³⁾ and succeeded in reducing the second-order inhomogeneity by about three times.^{10,11)} Although this method is simple and straightforward, correcting higher-order inhomogeneities, such as the third, fourth, and fifth orders, remains a challenge.

Recently, a flexible shimming method using circular coil arrays was proposed.^{12,13)} This approach facilitates correction of a complicated inhomogeneous magnetic field by driving a number of circular coils independently.

Here, we propose a novel design method for a single-channel shim coil for a narrow-gap permanent magnet based on the multicoil concept.

In our method, the current density \mathbf{J}_s for the single-channel shim coil is represented by the superposition of circular currents placed on an $n \times m$ square lattice, as shown in Fig. 1. The magnetic field B_s generated by the shim coil is

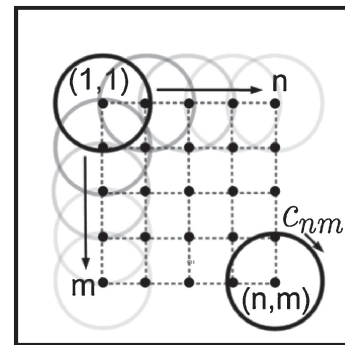


Fig. 1. Schematic diagram of the design method for the single-channel shim coil based on multiple circular currents.

a linear combination of the magnetic fields B_{nm} generated by circular currents:

$$B_s = \sum_n \sum_m c_{nm} B_{nm}, \quad (1)$$

where c_{nm} is the coefficient for the linear combination. The coefficients are determined using a nonlinear least-squares method (the Levenberg–Marquardt method¹⁴⁾) to fit B_s values to compensate for the inhomogeneous magnetic field (ΔB_z).

Then, \mathbf{J}_s is represented as

$$\mathbf{J}_s = \sum_n \sum_m c_{nm} (G(\sigma) * \mathbf{J}_{nm}), \quad (2)$$

where \mathbf{J}_{nm} is the current density at position (n, m) , $G(\sigma)$ is the normalized Gaussian filter with standard deviation σ , and $*$ denotes the convolution operation. \mathbf{J}_s is convoluted with $G(\sigma)$ to avoid abrupt changes in the current direction and undesirable higher-order spatial components of the magnetic field; σ is determined from a compromise between the performance of the shim coil and the difficulty of fabrication.

The winding pattern of the single-channel shim coil is derived using the stream function method from \mathbf{J}_s . The stream function Φ can be expressed as

$$\mathbf{J}_s = \nabla \times (\Phi \cdot \mathbf{n}), \quad (3)$$

where \mathbf{n} is the normal vector of the current surface. The winding pattern of the single-channel shim coil is obtained as the contour line of Φ .

Experiments were performed on a 1.0 T permanent magnet magnetic resonance imaging (MRI) system.¹⁵⁾ The

*E-mail address: tamada@mrlab.frsc.tsukuba.ac.jp

system was equipped with a planar gradient coil set, a radiofrequency (RF) probe with a solenoid coil, and an MRI console.

The specifications of the permanent magnet (NEOMAX Engineering) were magnetic field strength: 1.04 T; gap width: 90 mm, homogeneity: 10 ppm for a spherical volume, 30 mm in diameter, outer size: 57.4 cm (W) \times 52.0 cm (H) \times 48.0 cm (D), weight: 980 kg. Because the magnet was developed about 10 years ago, its homogeneity has decreased.

The magnetic field distribution B_z was measured using a three-dimensional (3D) lattice phantom consisting of 12 acrylic discs (3.0 mm thickness, 60.5 mm diameter) with square trenches (1.0 \times 1.0 mm² at 3.0 mm intervals) stacked in a cylindrical container (100 mm length, 60.6 and 65.0 mm, inner and outer diameters, respectively) filled with baby oil.^{16,17} The 3D images of the phantom were measured using 3D spin echo sequences [with 100 ms repetition time (T_R), 12 ms echo time (T_E), a matrix of 256 \times 256 \times 256, and (76.8 μ m)³ voxel size] with positive and negative readout gradients.

The spatial coordinates of the vertex points of the square lattice in the images were detected using a graphical user interface program. The magnetic field inhomogeneity ΔB_z at the vertex points in the central cylindrical area (54.6 mm diameter, 60.0 mm height) was calculated from the positional shifts of the vertices along the readout direction and was then approximated by fitting spherical harmonic functions up to the third order.

We optimized the current density of the single-channel shim coil to correct ΔB_z as measured in the central cylindrical area. The number of circular (25 mm diameter each) coils ($n \times m$) was 9 \times 9 and the number of contour lines was 40.

Figures 2(a) and 2(b) show the stream function Φ of J_s and the contour lines of Φ for the upper (a) and lower (b) sides of the shim coil, respectively.

The shim coil was fabricated on a 0.5-mm-thick fiber-reinforced plastic (FRP) square plate (200 \times 200 mm²) using polyethylene-coated Cu wires (0.5 mm diameter). Figures 2(c) and 2(d) show the fabricated upper- and lower-side shim coils, respectively. The total thickness of the fabricated shim coil was about 2 mm.

Figures 3(a) and 3(b) show the 3D magnetic field distribution over the cylindrical area measured without and with shimming using the single-channel shim coil, respectively. The inhomogeneous magnetic field [Fig. 3(a)] has clearly improved [Fig. 3(b)]. The magnetic field inhomogeneity was reduced from 240 to 97 ppm (peak-to-peak, PP) and from 24 to 10 ppm (root mean square, RMS).

Figures 4(a) and 4(b) show 2D cross-sectional images from 3D image datasets of a chemically fixed mouse acquired without and with the shim current using a 3D gradient echo sequence (with 100 ms T_R , 5 ms T_E , a matrix of 512 \times 128 \times 16, and 10.24 \times 2.56 \times 2.56 cm³ field of view), respectively. The magnetic field inhomogeneity caused undesirable intensity variations across the image [Fig. 4(a)]; however, the artifact was removed using the shim coil, as clearly shown in Fig. 4(b).

Figure 5 presents the magnetic field inhomogeneity vs the shim coil current. The triangles and circles indicate the RMS and PP values of the magnetic field inhomogeneity measured

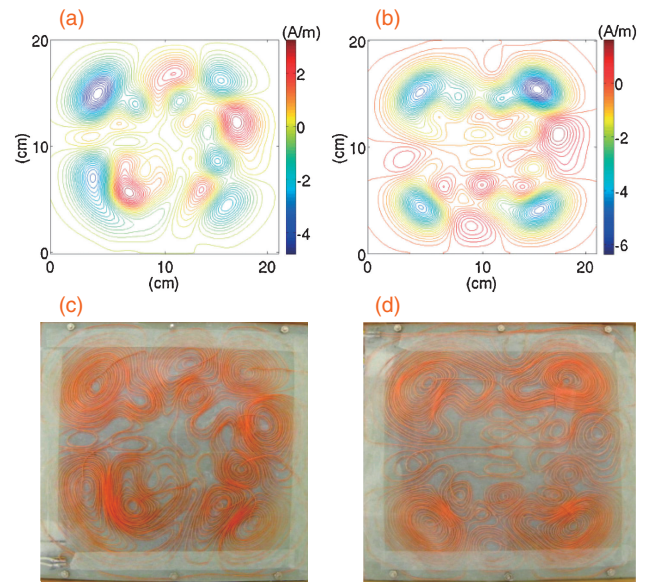


Fig. 2. Stream function Φ of J_s corresponding to the upper side (a) and lower side (b) of the single-channel shim coil. Contour lines show the winding pattern of the single-channel shim coil; (c) and (d) are the single-channel shim coils fabricated on the FRP plates corresponding to (a) and (b), respectively.

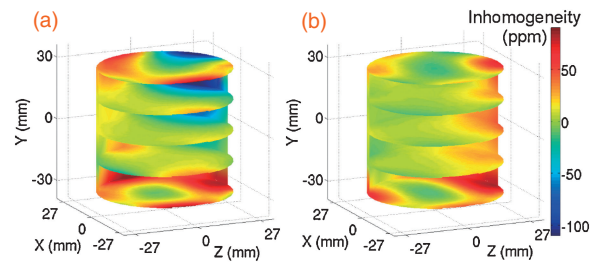


Fig. 3. Magnetic field distribution (a) without and (b) with shimming using the single-channel shim coil (SCSC).

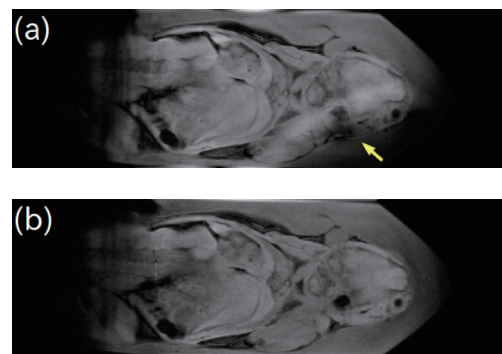


Fig. 4. 2D slices selected from 3D image datasets of a chemically fixed mouse acquired with a 3D gradient echo sequence: (a) without and (b) with shimming using the single-channel shim coil. The intensity variation indicated by the arrow is clearly improved.

in the experiment. The theoretical and experimental values are shown as red dashed and blue dotted lines, respectively. The RMS value was minimized when the shim coil current was around 1750 mA in the experiment, whereas the theoretical value was minimized when the shim coil current was around 2200 mA. This result can be explained from the

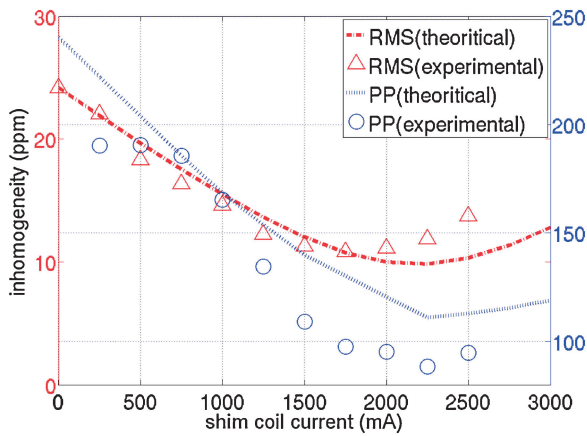


Fig. 5. Magnetic field inhomogeneity vs the shim coil current; the triangles and circles indicate RMS and PP values of magnetic field inhomogeneity obtained in the experiment, respectively. The red dashed and blue dotted lines, respectively, show the RMS values and PP values of the magnetic field inhomogeneity calculated using Biot–Savart’s law.

effect of the pole piece,¹⁸⁾ which is the widely known phenomenon whereby the magnetic field induced by a coil mounted near the pole piece is significantly enhanced because of the mirror current effect.

The magnitude of the second-order term was reduced from 112 to 43 ppm (PP) and from 18 to 6.2 ppm (RMS), respectively. The magnitude of the third-order terms was also reduced from 61 to 25 ppm (PP) and from 7.6 to 3.5 ppm (RMS), respectively. The results show our approach is effective to improve higher-order inhomogeneities.

Several critical design parameters should be carefully determined for the single-channel shim coil. These are the size of the coil array, the diameter of the circular currents, the width of the Gaussian convolution function represented by the standard deviation σ , and the number of turns of the coil.

A larger coil array size would improve the correction accuracy for the magnetic field inhomogeneity. However, because the calculation time for current density optimization increases dramatically with the coil array size, we used a 9×9 array. If we had used a much faster computation system, calculation for a larger coil array would have been possible.

The diameter of circular currents is an important parameter in the design of less complicated winding patterns. The current density distribution of the shim coil becomes more complicated as the diameter of the circular currents becomes smaller because small circular currents make the high-density area and produce hot spot. Hence, it is desirable to use circular currents with a diameter as large as possible to avoid the above problem. However, the diameter of the circular current coils is limited by the total size of the shim coil, about 200 mm^2 . Therefore, we performed calculations for several coil diameters and selected 25 mm.

The width of the Gaussian convolution function represented by the standard deviation σ is a critical factor that determines the accuracy of the field correction. If we use a smaller σ , or a narrower Gaussian filter, both the current density and wire pattern change very steeply. On the other hand, if we use a larger σ , or a wider Gaussian filter, it is

difficult to correct the inhomogeneous magnetic field sufficiently. Therefore, we repeated the calculation for several σ values and selected $\sigma = 13 \text{ mm}$.

Using a larger number of turns of the coil improves the approximation for continuous current density. In addition, having a larger number of turns decreases the effectiveness of unfavorable magnetic fields produced by the wires connecting the circular currents. However, a larger number of turns corresponds to a smaller diameter of the coil wire, which produces considerable Joule heat. We therefore used 40 turns.

The diameter of the wires is a critical factor to determine the power consumption of the shim coil. The power consumption is important because it affects the magnet temperature. In order to minimize the power consumption, it is desirable to use larger diameter wires. In this study, we used 0.5 mm diameter wires. As a result, the power consumption of the shim coil was about 7 W, acceptable level.

Our method is simple and has a comparative advantage over the target-field method. The coil design using the target-field is one of the useful methods for shim coil design however sometimes troublesome because it is difficult to select the target-field points properly when the target field is complicated. On the other hand, our method is more straightforward for a magnet, whose magnetic field includes higher-order inhomogeneities.

In this study, we designed and fabricated a planar single-channel shim coil for a permanent magnet with 1.0 T and a 90 mm gap. As a result, the magnetic field inhomogeneity in the central cylindrical area was improved by a factor of about 2.5. In conclusion, the planar single-channel shim coil based on the multiple circular-coil concept is a useful device for narrow-gap permanent magnets with a complicated inhomogeneous magnetic field.

Acknowledgment We are very grateful to Dr. Y. Terada for his useful advice.

- 1) D. I. Hoult and D. Lee: *Rev. Sci. Instrum.* **56** (1985) 131.
- 2) M. J. E. Golay: *Rev. Sci. Instrum.* **29** (1958) 313.
- 3) F. Roméo and D. I. Hoult: *Magn. Resonance Med.* **1** (1984) 44.
- 4) W. A. Anderson: *Rev. Sci. Instrum.* **32** (1961) 241.
- 5) R. Shigeki and K. Kose: *Proc. Int. Soc. Magn. Resonance Med.* **19** (2010) 1542.
- 6) R. Turner: *Magn. Resonance Imaging* **11** (1993) 903.
- 7) M. A. Martens, L. S. Petropoulos, R. W. Brown, J. H. Andrews, M. A. Morich, and J. L. Patrick: *Rev. Sci. Instrum.* **62** (1991) 2639.
- 8) S. Crozier, S. Dodd, K. Luescher, J. Field, and D. M. Doddrell: *Magn. Resonance Mater. Phys. Biol. Med.* **3** (1995) 49.
- 9) M. Engelsberg, R. E. D. Souza, and C. M. D. Pazos: *J. Phys. D* **21** (1988) 1062.
- 10) D. Tamada, Y. Terada, and K. Kose: *Appl. Phys. Express* **4** (2011) 066702.
- 11) Y. Terada, D. Tamada, and K. Kose: *J. Magn. Resonance* **212** (2011) 355.
- 12) C. Juchem, T. W. Nixon, S. McIntyre, D. L. Rothman, and R. A. de Graaf: *J. Magn. Resonance* **204** (2010) 281.
- 13) C. Juchem, T. W. Nixon, S. McIntyre, V. O. Boer, D. L. Rothman, and R. A. de Graaf: *J. Magn. Resonance* **212** (2011) 280.
- 14) J. Moré: *J. Numer. Anal.* **630** (1978) 105.
- 15) T. Shirai, T. Haishi, S. Utsuzawa, Y. Matsuda, and K. Kose: *Magn. Resonance Med. Sci.* **4** (2005) 137.
- 16) D. Wang, D. M. Doddrell, and G. Cowin: *Magn. Resonance Imaging* **22** (2004) 529.
- 17) S. Adachi, T. Ozeki, R. Shigeki, S. Handa, K. Kose, T. Haishi, and M. Aoki: *Rev. Sci. Instrum.* **80** (2009) 054701.
- 18) C. H. Moon, H. W. Park, and S. Y. Lee: *Meas. Sci. Technol.* **10** (1999) 136.